Isı Bilimi ve Tekniği Dergisi, 29, 1, 55-65, 2009
J. of Thermal Science and Technology

ISSN 1300-3615

NATURAL CONVECTION HEAT TRANSFER FROM A THIN HORIZONTAL ISOTHERMAL PLATE IN AIR-FILLED RECTANGULAR ENCLOSURES

Zekeriya ALTAÇ* and Seda KONRAT**

*Eskişehir Osmangazi University, School of Engineering and Architecture, Mechanical Engineering Department, Batı-Meşelik, 26480, Eskişehir, zaltac@ogu.edu.tr
**TEI Tusaş Engine Industries Inc., Muttalip Mevkii, 26000 Eskişehir, sedakonrat@yahoo.com

(Geliş Tarihi: 09. 09. 2008, Kabul Tarihi: 05. 01. 2009)

Abstract: An air filled rectangular enclosure containing an isothermal plate is cooled from a lateral wall while other three sides are insulated. A horizontally situated thin isothermal plate is the sole source of heat input within the system. The plate and the cold walls are maintained at constant temperatures. The transport equations, along with the Boussinesq approximation as well as the energy equation, are solved using the finite volume method (FVM) coupled with SIMPLE algorithm. The steady state mean Nusselt number over the isothermal plate surface area is computed for each case as a function of Rayleigh number, the plate length and position. Rayleigh number is varied from 10^5 to 5×10^7 while two plate length alternatives were studied—50% and 75% of the enclosure length. The plate thickness was kept constant—1% of the enclosure height. The effects of the plate length, the plate position and the aspect ratio (A=1 and 2) on the heat transfer characteristics and the fluid flow were investigated. For increasing Rayleigh number the heat transfer rates increases, and for increasing plate length the heat transfer rate (Nusselt number) decreases by about 25%. As a result of the numerical parametric study, a correlation for the Nusselt number is obtained to be used for practical cooling problems.
Keywords: Natural convection, Laminar flow, Rectangular enclosures, Isothermal plate, Horizontally located

HAVA DOLU KAPALI KUTULAR İÇİNDEKİ BİR İNCE YATAY İZOTERMAL PLAKADAN DOĞAL TAŞINIM İLE ISI GEÇİŞİ

Özet: Bir izotermal plaka içeren hava dolu dikdörtgensel kapalı kutunun diğer üç kenarı yalıtılmış iken bir dikey kenarından soğutulmaktadır. Yatay olarak konumlandırılan izotermal plaka sisteme ısı girişinin tek kaynağıdır. Plaka ve soğuk duvarlar sabit sıcaklıkta muhafaza edilmektedir. Boussinesq yaklaşımı ile beraber taşınım denklemleri ve enerji denklemi SIMPLE algoritması ile kuple edilen sonlu hacim metodu (FVM) kullanılarak çözülmektedir. Sürekli rejimde, izotermal plaka yüzey alanı üzerinden ortalanan Nusselt sayısı, Rayleigh sayısı, plaka uzunluğu ve konumunun bir fonksiyonu olarak hesaplanmıştır. Rayleigh sayısı 10^5 ile 5×10^7 arasında değiştirilirken, kutu uzunluğunun %50 ve %75'ine varan iki plaka uzunluğu alternatifi göz önüne alınmıştır. Plaka kalınlığı kutu yüksekliğinin %1'i olarak sabit tutulmuştur. Plaka uzunluğu, plaka konumu ve incelik oranının (A=1 ve 2) ısı transfer karakteristikleri ve akışkan akışına etkileri incelenmiştir. Artan Rayleigh sayısı ile ısı geçiş oranı artmaktadır ve artan plaka uzunluğu ile ısı geçiş oranı (Nusselt sayısı) yaklaşık %25 azalmaktadır. Bu sayısal parametrik çalışmanın bir sonucu olarak, pratik soğutma problemlerinde kullanmak üzere, bir Nusselt sayısı bağıntısı elde edilmiştir.
Anahtar Kelimeler: Doğal taşınım, Laminer akış, Kapalı kutular, İzotermal plaka, Yatay konum

INTRODUCTION

Natural convection in fluid-filled enclosures has received considerable attention in recent years since this phenomenon often affects the thermal performance of various systems. Buoyancy-driven flows have many applications in thermal engineering since passive cooling of electronic components by natural convection is the least expensive, quietest and most reliable method of heat rejection alternative. Among these applications involving enclosures are electronic packages of computer components, solar collectors and energy storage systems. Under certain circumstances electronic components are packaged within sealed enclosures, while one or more of the walls are cooled. The main source of heat within the enclosures is electronic components and/or boards situated in various configurations.

A number of studies on convection cooling applicable to thermal control of electronic equipment were reviewed by Incropera (1988). Laminar and turbulent natural convection heat transfer from rectangular enclosures that are heated and cooled from lateral wall has been extensively examined. In the last decade, the attention

has shifted to the study of natural convection in partitioned enclosures and enclosures with discrete heat sources attached to its adiabatic walls. On the other hand, natural convection from heated elements within enclosures has received almost no attention until very recently. Sun and Emery (1997) numerically studied two-dimensional conjugate natural convection heat transfer in an enclosure containing discrete internal heat sources and an internally conducting baffle. Dağtekin and Öztop (2001) numerically studied the natural convection heat transfer and fluid flow of two heated partitions in a rectangular enclosure for Rayleigh number range of 10^4-10^6. The partitions', attached to the bottom wall, the length and the location were varied while the enclosure was cooled from two walls.

A numerical study of laminar natural convection from a two dimensional horizontal channel with rectangular heated blocks was performed by Alami et al. (2005). Bessaih and Kadja (2000) studied numerical simulation of conjugate turbulent natural convection air cooling of three heated-ceramic components, mounted on a vertical adiabatic channel. An experimental and numerical investigation on the effect of the position of the wall mounted blocks on the heat transfer, accounting for the angular displacement of the block, was performed by Bilen et al. (2001). Sathe and Joshi (1990) studied numerically heat dissipation by natural convection from a heat generating protrusion, mounted on a substrate inside a square enclosure. Ben-Nakhi and Chamkha (2006) numerically investigated natural convection heat transfer from an inclined heat fin attached to the hot wall of a square enclosure. Frederick and Valencia (1989) studied the heat transfer in a square cavity with a conducting partition on its hot wall.

Heindel et al. (1995) performed 2D and 3D numerical simulations of laminar flow induced by a 3×3 array of discrete heat sources mounted to a vertical wall of a rectangular cavity whose opposite wall was cooled. In a companion paper (1995) on 3D numerical simulation compared well with experimental data, and heat transfer correlations were developed. Desai et al. (1995) considered rectangular enclosures with multiple heaters mounted on one side wall, with the top wall being cooled while the other walls were insulated. Their predictions also compared well with previous experimental and numerical work. Kang and Jaluria (1990) experimentally studied the heat transfer from a heat source module of finite thickness, mounted on a vertical or horizontal wall. Their results indicate that the natural convection flow and the associated heat transfer characteristics varied strongly with the rate of energy input and the source thickness. Türkoğlu and Yücel (1996) numerically analyzed 2D flow and heat transfer in enclosures with conducting multiple partitions. They observed that the mean Nusselt number decreased with increasing number of partitions, and the aspect ratio did not affect the mean Nusselt number. Yücel and Türkoğlu (1998) also numerically studied fluid flow and heat transfer in partially divided square enclosures. It was observed that the mean Nusselt number increased with increasing Rayleigh number and decreased with increasing number of partitions; however, the decline in the mean Nusselt number was much less at low Rayleigh numbers. Increasing the partition height resulted in a decrease in the mean Nusselt number.

Barozzi et al (1999) investigated 2D buoyant flow in an air-filled enclosure, containing two parallel vertically heated plates. Two cases, isothermal and uniform heat generation, were considered for Grashoff number 10^5 and 10^7. Transient and long term thermal and flow behavior were investigated. In an extension, Barozzi and Corticelli (2000) performed 2D numerical simulation of two vertical plates with uniform heat generation and a rectangular heating block with uniform wall temperature, placed at the center of the enclosure. The air-filled cavity was cooled by the vertical walls. Grashoff number was varied from 4×10^4 to 10^8. Bilgen (2005) numerically studied 2D square differentially heated cavities, with a thin fin is attached on the active wall. The effects of Rayleigh number (10^4 to 10^9), dimensionless thin fin length (0.10 to 0.90), dimensionless thin fin position (0 to 0.90), dimensionless conductivity ratio (0 to 60) were examined. It is found that Nusselt number increased with Rayleigh number and decreased with fin length and conductivity ratio, and an optimum fin position existed. Altaç and Kurtul (2007) numerically studied 2D natural convection in tilted rectangular enclosures with a vertically situated hot plate placed at the center. The plate was very thin and isothermal. The enclosure was cooled from a vertical wall only. Rayleigh numbers and the tilt angles of the enclosure ranged from 10^5 to 10^7 and from 0 to 90 degrees. The flow pattern and temperature distribution were analyzed, and steady-state plate-surface-averaged Nusselt numbers were correlated.

The motivation of the present work is the heat transfer from electronic equipments in a rectangular packaging enclosures containing air (Pr=0.7). This study differs from previously studies in that a heat generating plate simulating an electronic board mounted perpendicular to rectangular cross section in various horizontal locations. The effects on the flow and heat transfer characteristics for Rayleigh number ranging from 10^5 to 5×10^7, for the isothermal plate length ranging from $0.5L$ to $0.75L$ and for aspect ratio of A=1 and 2 are investigated parametrically.

MATHEMATICAL FORMULATION

Natural convection heat transfer from a horizontal isothermal plate of length ℓ is placed inside a rectangular enclosure of height H and length L. The geometry and the coordinate system are illustrated in Figure 1. The plate thickness is assumed to be constant ($\delta=0.01H$). The source strength of the system is

represented by both lower and upper walls of the isothermal plate (2 ℓ) which are kept at T_h temperature. Cooling is provided from the cold lateral wall (T_c) only, and the rest of the walls within the enclosure are adiabatic.

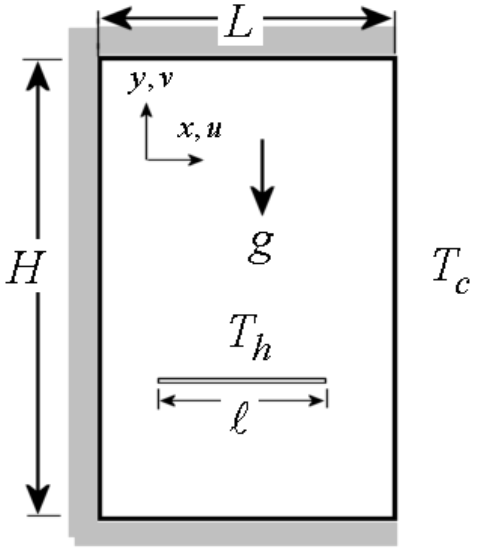

Figure 1. Geometry and coordinate system.

Two-dimensional continuity, transient momentum and energy equations using the Boussinesq approximation are numerically solved. The momentum equations are expressed in terms of vorticity and stream function formulations. The dimensionless form of the governing equations can be cast as;
for the vorticity

$$\frac{\partial\zeta}{\partial\tau}+\frac{\partial}{\partial X}(U\zeta)+\frac{\partial}{\partial Y}(V\zeta)=\sqrt{\frac{\Pr}{Ra}}\left(\frac{\partial^2\zeta}{\partial X^2}+\frac{\partial^2\zeta}{\partial Y^2}\right)-\frac{\partial\theta}{\partial X} \quad (1)$$

for the energy

$$\frac{\partial\theta}{\partial\tau}+\frac{\partial}{\partial X}(U\theta)+\frac{\partial}{\partial Y}(V\theta)=\frac{1}{\sqrt{Ra\,\Pr}}\left(\frac{\partial^2\theta}{\partial X^2}+\frac{\partial^2\theta}{\partial Y^2}\right) \quad (2)$$

and for the stream function

$$\frac{\partial^2\Psi}{\partial X^2}+\frac{\partial^2\Psi}{\partial Y^2}=-\zeta \quad (3)$$

where the velocity components and the vorticity are defined as

$$U=\frac{\partial\Psi}{\partial Y},\quad V=-\frac{\partial\Psi}{\partial X},\quad \zeta=\frac{\partial V}{\partial X}-\frac{\partial U}{\partial Y} \quad (4)$$

In deriving Equations (1)-(4), the following dimensionless variables were introduced:

$$(X,Y)=\frac{(x,y)}{H},\quad (U,V)=\frac{(u,v)}{(\alpha/H)\sqrt{Ra\,\Pr}},$$
$$\tau=\frac{\alpha\sqrt{Ra\,\Pr}}{H^2}t,\qquad \Psi=\frac{\psi}{\alpha\sqrt{Ra\,\Pr}} \quad (5a)$$

$$\theta=\frac{T-(T_h+T_c)/2}{T_h-T_c},\quad P=\frac{H^2}{\rho\alpha^2}\left(\frac{p+\rho gy}{\mathrm{Ra}\,\Pr}\right),$$
$$\mathrm{Ra}=\frac{g\beta(T_h-T_c)H^3}{\alpha\nu} \quad (5b)$$

where Ra and Pr are Rayleigh and Prandtl numbers, respectively.

The enclosure is filled with motionless fluid at a uniform θ=0 initial temperature, and it is assumed that all walls are impermeable no-slip boundaries. The boundary conditions can be stated as for

the right wall:

$U=V=0,\ \theta=-0.5$ for $X=1/A$

for the hot plate surfaces:

$$U=V=0,\quad \theta=0.5\ \text{ for }\ \frac{1}{2A}\left(1-\frac{\ell}{L}\right)\le X\le\frac{1}{2A}\left(1+\frac{\ell}{L}\right)$$

and for the other walls: $U=V=0,\ \dfrac{\partial\theta}{\partial n}=0$

where n is the normal direction of a surface, and A is the aspect ratio of the enclosure defined as $A=H/L$.

The mean Nusselt number for the isothermal plate surfaces is computed as

$$\mathrm{Nu}=-\frac{A/2}{\ell/L}\int_{X=(1-\ell/L)/2A}^{(1+\ell/L)/2A}\left\{\left.\frac{\partial\theta}{\partial Y}\right|_{\text{bottom}}+\left.\frac{\partial\theta}{\partial Y}\right|_{\text{upper}}\right\}dX \quad (6)$$

Equations (1)-(4) were solved numerically using Finite Volume Method (FVM) described by Patankar (1980). Starting with an initial velocity profile and using general transport equation for property ϕ where ϕ represents here vorticity and dimensionless temperature, Equations (1) and (2) are solved using the SIMPLE algorithm. Then the stream function is obtained from the solution of equation (3). The velocity components for the next time step are obtained from equation (4). Power-Law scheme for evaluation of the convection terms and the tridiagonal matrix algorithm in solving the finite-difference equations were adapted. Non-uniform rectangular grid structures condensed near the solid walls was adapted where sharp velocity and temperature gradients are expected. A computer code was developed and verified for the rectangular enclosures. In Table 1, the mean Nusselt number computed by 100×100 and 200×200 uniform grid configurations for a square cavity which is heated and cooled from the lateral walls are compared with other works [21-24]. This comparison indicated that 200×200 grid (or 40,401 nodes) yielded, for the mean Nusselt values, results with less than 1% deviation from the other works. In the presented geometry, the enclosure with an isothermal plate, the condensed grid near the isothermal plate yielded 65,119 nodes for square and 93,675 nodes for rectangular (A=2) enclosures.

Table 1. Computer code results in comparison with other works.

Ra Number	Mean Nusselt Number					
	Markatos& Pericleous (1984)	Vahl Davis (1983)	Le Quéré (1991)	Comini et al. (1995)	This Study	
					100×100	200×200
10^3	1.108	1.118			1.1064	1.1098
10^4	2.201	2.243			2.2273	2.2396
10^5	4.430	4.519		4.503	4.4877	4.4981
10^6	8.754	8.799	8.825	8.825	8.755	8.804
10^7			16.523	16.533	16.422	16.467
10^8	32.045		30.225	30.161	30.285	30.072

RESULTS AND DISCUSSION

In this study, enclosures with aspect ratios of A=1 and 2, containing air (Pr=0.7), are considered. The isothermal plate locations, $Y_0=y_0/H$=0.25, 0.50 and 0.75, and two plate length alternatives of ℓ =0.5L and ℓ =0.75L are studied. Numerical computations were carried out for the following Rayleigh numbers: 10^5, 5×10^5, 10^6, 5×10^6, 10^7 and 5×10^7.

Square Enclosures

In Figure 2, for three plate locations, the temperature and flow fields for A=1, ℓ=0.5L, Ra=10^5, 10^6 and 10^7 are depicted. In Figures 2(a), 2(b) and 2(c), for Y_0=0.25 plate location, thermal boundary layers at the lower and upper surfaces of the plate and the thickness of the plume in which hot fluid is rising thin out for increasing Rayleigh number, resulting in increased heat transfer rates. The main circulation encircles the plate. Formation of a second, weaker, counter-clockwise circulation in the upper left corner of the enclosure, Figure 2(a), is responsible for pushing the plume towards the cold wall. For Ra=10^6, the main circulation still encloses the isothermal plate while the weaker counter-clockwise circulation at the upper-left corner of the enclosure slightly gains strength. In Figure 2(b), the main circulation takes the form of an L-shape, while a roll inside the main circulation—between the plate and the cold wall—develops and gains strength with increasing Rayleigh number as seen in Figure 2(c). For Ra=10^7, the inner roll within the main circulation is especially distorted along the cold wall due to descending fluid adjacent to the cold wall. With increasing Rayleigh number, the temperature gradients along the hot and cold walls become steeper. In Figures 2(d), 2(e) and 2(f), the isotherms and streamlines for the isothermal plate which is located in the middle of the enclosure (Y_0=0.5) is depicted. The thermal boundary layer around the plate and cold wall and the hydrodynamic boundary layer near the cold wall thin out with increasing Rayleigh number, extending down to the horizontal level of the plate. The main circulation shifts towards the cold wall, and gets elongated between the plate and the cold wall while the core remains in the upper right corner of the enclosure—Figure 2(e). As Rayleigh number is increased to 10^7, the main circulation is confined between the plate and the cold wall occupying upper-right corner of the enclosure Figure 2(f). Temperature and velocity gradients increase around the plate walls and the cold wall with increasing Rayleigh number. In Figures 2(g), 2(h) and 2(i), the isothermal plate is shifted vertically up to Y_0=0.75 location. Both hydrodynamic and thermal boundary layers are thin at the upper portion of the cold wall for all Rayleigh cases. For Ra=10^5, Figure 2(g), the main roll encircles the plate while the core of the central roll remains below the plate, leaning towards the cold wall. However, as Rayleigh number is increased to Ra=10^6, the central circulation migrates towards the upper right corner of the enclosure, Figure 2(h), due to faster moving fluid pushing weaker central roll upwards. Dense isotherms are established at the upper one-third of the cold wall, and a weak counterclockwise roll, at the upper left corner, accompanies the main roll. This indicates that the heat transfer rate decreases as the isothermal plate location is vertically elevated within the enclosure.

In Figure 3, for three plate locations, the temperature and flow fields for A=1, ℓ /L=0.75, Ra=10^5, 10^6 and 10^7 are shown. For the plate location Y_0=0.25, in Figures 3(a), 3(b) and 3(c), for increasing Rayleigh number, distinct thermal boundary layers are observed at the bottom wall of the isothermal plate and along the cold wall starting from the top all the way to the bottom. The boundary layer thicknesses, including the top wall of the plate, become thinner for increased Rayleigh number. For Ra=10^5, Figure 3(a), a main roll encloses the isothermal plate, and inside the main circulation, a second unicellular roll above the plate is established. The main circulation which takes inverted L-shape gains strength, and the central roll first loses strength, Figure 3(b), then as Rayleigh number increases, two weak rolls located above and below the plate are established in the vicinity of the cold wall which are then combined to form a squeezed roll (Figure 3(c)). The hot plume rises from the plate along the fastest moving streamlines which are pushed towards the cold wall due to expanding counter clock-wise circulation on the upper left corner of the enclosure (Figure 3(b) and 3(c)). The location of the plume on the plate shifts towards the cold wall with increasing Rayleigh. In Figures 3(d), 3(e) and 3(f), the isothermal plate is placed

in the middle of the enclosure. The main circulation encompasses the isothermal plate for all Rayleigh cases. In addition to the main roll, for Ra=10^5 in Figure 3(d), two smaller also clockwise rotating rolls appear below and above the plate. In Figure 3(e), as Rayleigh number is increased to 10^6, the circulation above the plate gains while the one at the bottom loses its strength; on the other hand, the roll at the upper left corner expands. Figure 3(f), for Ra=10^7, both rolls combine and occupy a large portion of the upper-right corner of the enclosure stretching along the cold wall and passing through the gap between the plate and the cold wall. Steep temperature and velocity gradients are clearly visible for Ra=10^6 and 10^7 occurring mainly all around the plate (much denser at the bottom wall) and the cold wall extending down to the horizontal level of the plate. In Figures 3(g), 3(h) and 3(i), the isotherms and the streamlines for the plate which is located at Y_0=0.75 are given. The main circulation still encompasses the isothermal plate for all Rayleigh cases; however, as seen in Figure 3(g), inside the main circulation, a roll located below the plate is stronger. In Figure 3(h), the two circulations, above and below the plate, combine to form a single roll for Ra=10^6; however, two frail rolls still exist inside this stretched roll.

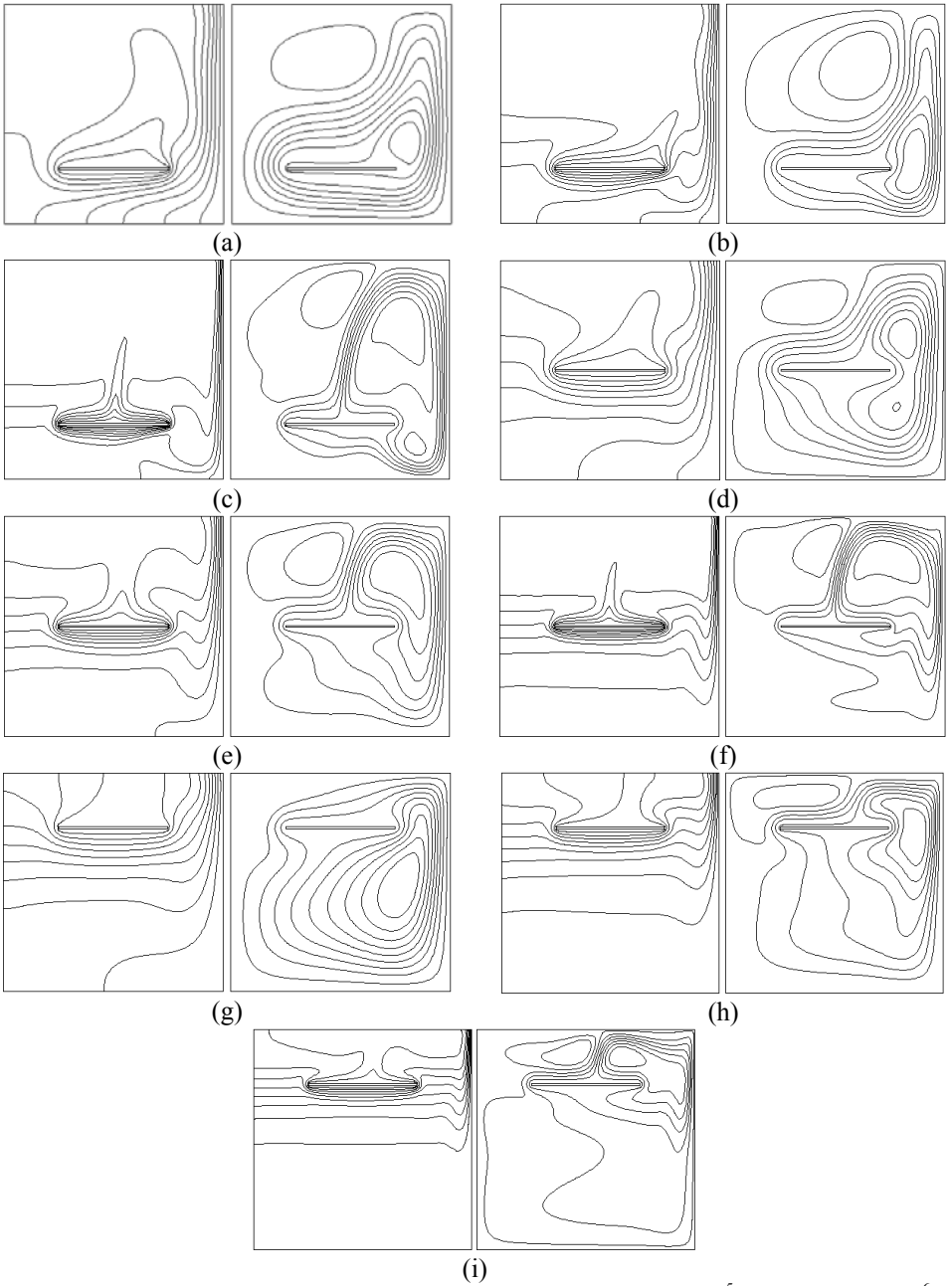

Figure 2. Isotherms (left) and streamlines (right) for A=1 and ℓ =0.5L, (a), (d), (g) Ra=10^5; (b), (e), (h) Ra=10^6; and (c), (f), (i) Ra=10^7 (For (a), (b), (c) Y_0=0.25, for (d), (e), (f) Y_0=0.5, and for (g), (h), (i) Y_0=0.75).

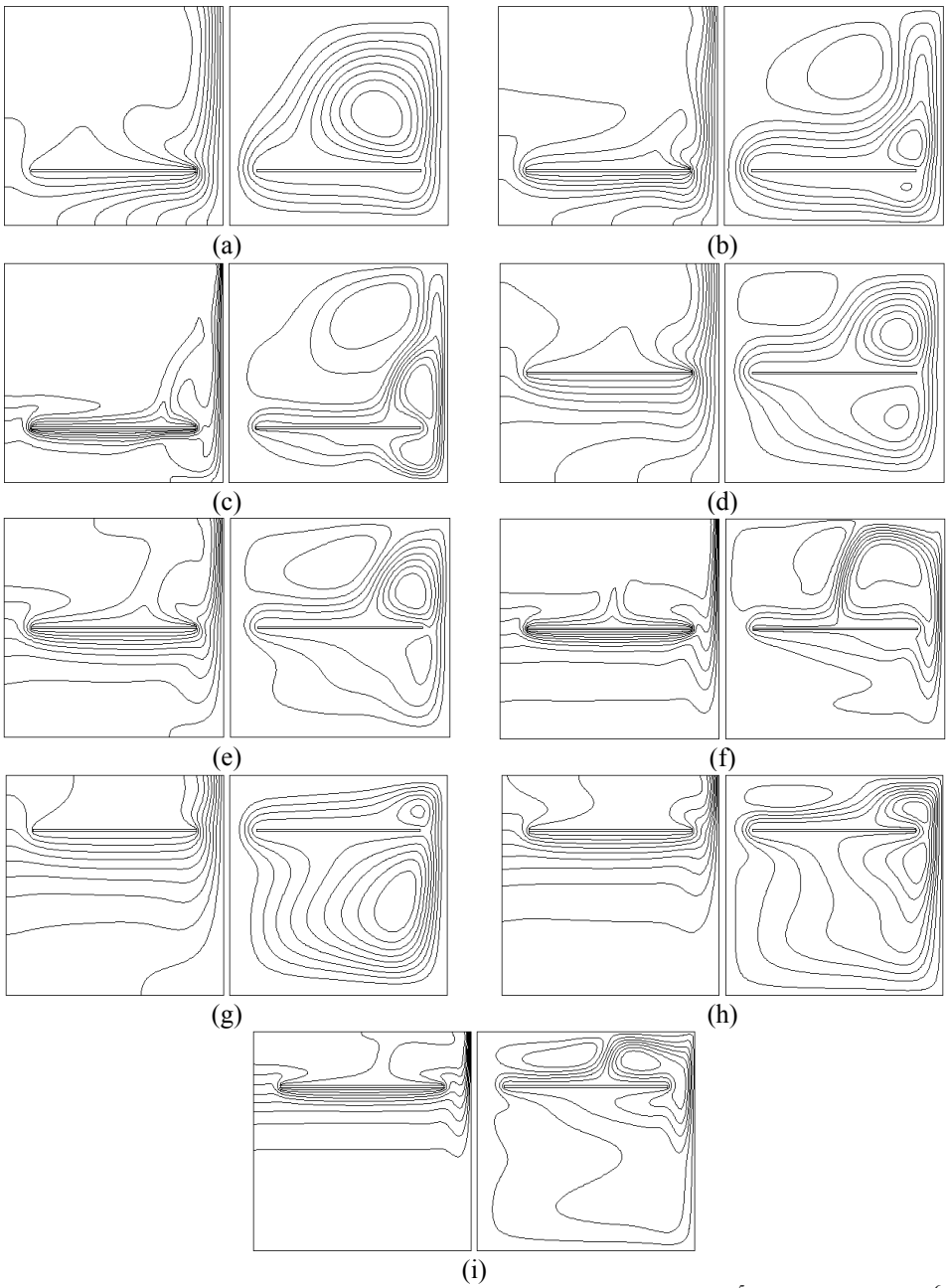

Figure 3. Isotherms (left) and streamlines (right) for A=1 and ℓ/L=0.75, (a), (d), (g) Ra=10^5; (b), (e), (h) Ra=10^6; and (c), (f), (i) Ra=10^7 (For (a), (b), (c) Y_0=0.25, for (d), (e), (f) Y_0=0.5, and for (g), (h), (i) Y_0=0.75).

Finally, for Ra=10^7 in Figure 3(i), the central roll is confined to the upper-right corner of the enclosure. For increasing Rayleigh number, a weak counter-clock wise roll at the upper left corner of the plate causes the plume to rise to the top wall of the enclosure. Both thermal and hydrodynamic boundary layers are clearly observed along the cold wall which run from the top of the enclosure to the horizontal plate level whereas the thermal boundary layer below the plate and hydrodynamic boundary layer above the plate are distinct. Both boundary layer thicknesses further thin out with increasing Rayleigh number.

In Figure 4, the local Nusselt number ($Nu_X=-\partial\theta/\partial Y$) variation along the top and bottom walls of the isothermal plate (ℓ/L=0.5) located at Y_0=0.5 of A=1 enclosure is plotted for Ra=10^5, 10^6 and 10^7. Under the plate, a very low velocity flow creates two boundary layers starting from the center of the plate and going to the edge to meet the upper flow. For Ra=10^5, the local Nusselt number of along the bottom wall is nearly flat but dramatically increases towards the edges of the plate where temperature gradients are steeper. The formation of boundary layers on top wall of the plate, starting from the edges, converges near the center of the plate forming laminar vertical plume attached to the plate. In Figure 2(d) for Ra=10^5, the plume is thick and has a wide base area on the isothermal plate. For increasing Rayleigh number, the location of the plume detaching from the top wall shifts towards the middle of the plate as it becomes slender in shape. The heat transfer inside

the base of detaching plume corresponds mainly to conduction regime associated with a very weak flow; therefore, the heat transfer from the top wall is lower. For increasing Rayleigh number, the heat transfer rate from the bottom wall steadily increases while the local Nusselt number remaining almost flat for most of the portion of the bottom wall. On the other hand, the heat transfer rate from the top wall also increases while the conducting base area of the plume shrinks and shifts to the middle of the plate due to expanding counter-clockwise rolls (Figure 2(f)).

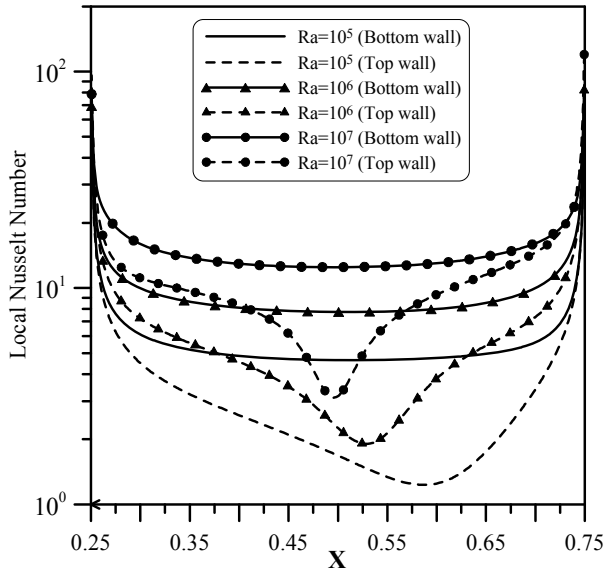

Figure 4. Local Nusselt number variation along the top and bottom walls of the isothermal plate as a function of Rayleigh number for A=1, Y_0=0.5 and ℓ /L=0.5 case.

Rectangular Enclosures (A=2)

In Figure 5, the isotherms and streamlines for A=2, ℓ /L=0.5, Ra=10^5, 10^6 and 10^7 are given for three plate locations. When the plate is located at Y_0=0.25 for Ra=10^5 in Figure 5(a), the main clock-wise circulation runs around the plate which contains another strong unicellular roll above the plate. The hot plume rises towards the upper-left corner of the enclosure along the interface of the outer and inner rolls. As Rayleigh number is increased to 10^6, in the vicinity of the cold wall, Figure 5(b), the unicellular circulation is broken up into two clockwise rolls above and a weak one below the isothermal plate. On the other hand, at the upper-left corner of the enclosure, formation of a weak counter-clock-wise roll pushes the plume towards the cold wall. The thermal boundary layers around the plate become thinner as Rayleigh number increases, yielding an increase in the heat transfer rates from the plate. In Figure 5(c), the counter-clock wise roll on the upper left corner of the enclosure gains strength as it expands. The isotherms exhibit slender thermal boundary layers around the plate and along the cold wall starting from the top all the way down to the horizontal plate level. The streamlines shrink to cover the plate tightly.

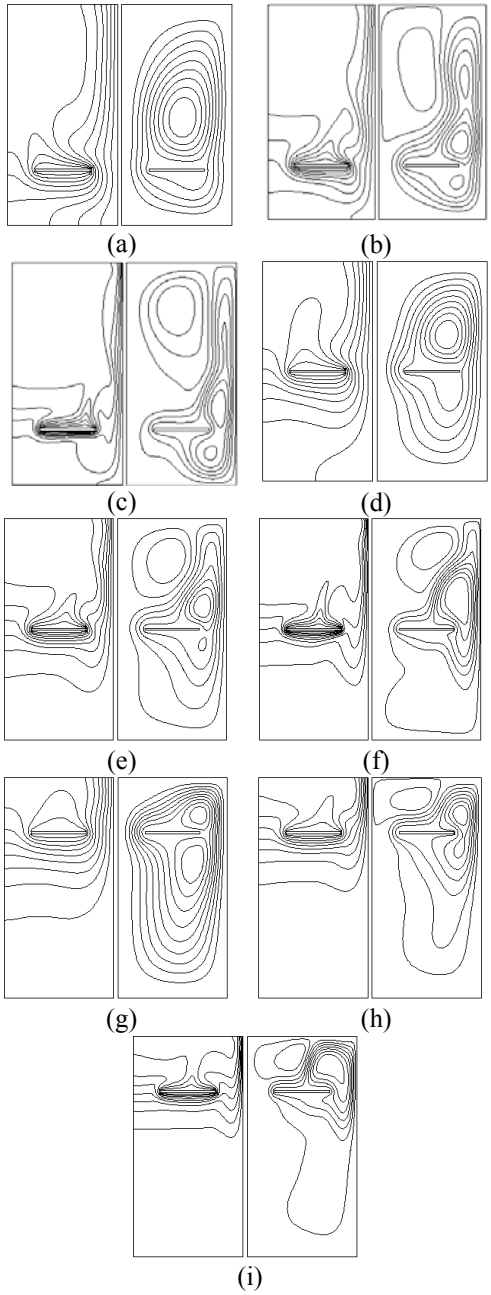

Figure 5. Isotherms (left) and streamlines (right) for A=2 and ℓ /L=0.5, (a), (d), (g) Ra=10^5; (b), (e), (h) Ra=10^6; and (c), (f), (i) Ra=10^7 (For (a), (b), (c) Y_0=0.25, for (d), (e), (f) Y_0=0.5, and for (g), (h), (i) Y_0=0.75).

For increasing Rayleigh number, the plume location on top wall moves from left to right. The isotherms and streamlines for the plate which is located at the middle of the enclosure are depicted in Figures 5(d), 5(e), 5(f). The streamlines are similar to Y_0=0.25 cases; however, the second counter-clock-wise circulation on the upper left corner is smaller. For Ra=10^5, a second roll within the main circulation is at first unicellular, but for increasing Rayleigh number, it stretches along the cold wall and the plate—Figure 5(f), For high Rayleigh flows, a frail counter-clock-wise roll on the upper left corner is consistently obtained (Figs. 5(b), 5(c), 5(e) and 5(f)). Sharp temperature gradients along the cold wall extends from the top of the enclosure to the plate levels

indicating lesser heat transfer rate from the enclosure in comparison to the plate position of Y_0=0.25 case. In Figure 5(g), a flow pattern which becomes typical of Y_0=0.75 location is observed; that is, two weaker rolls within the main roll are separated by the plate. These rolls combine to form another clockwise roll while a counter-clockwise roll on the upper left corner pushes the plume towards the cold wall (Figure 5(h)). As the combined roll moves to occupy the upper right corner of the enclosure, it stretches along the gap between the cold wall and the plate. The streamlines and isotherms on the cold wall are dense and stacked up at the horizontal plate level.

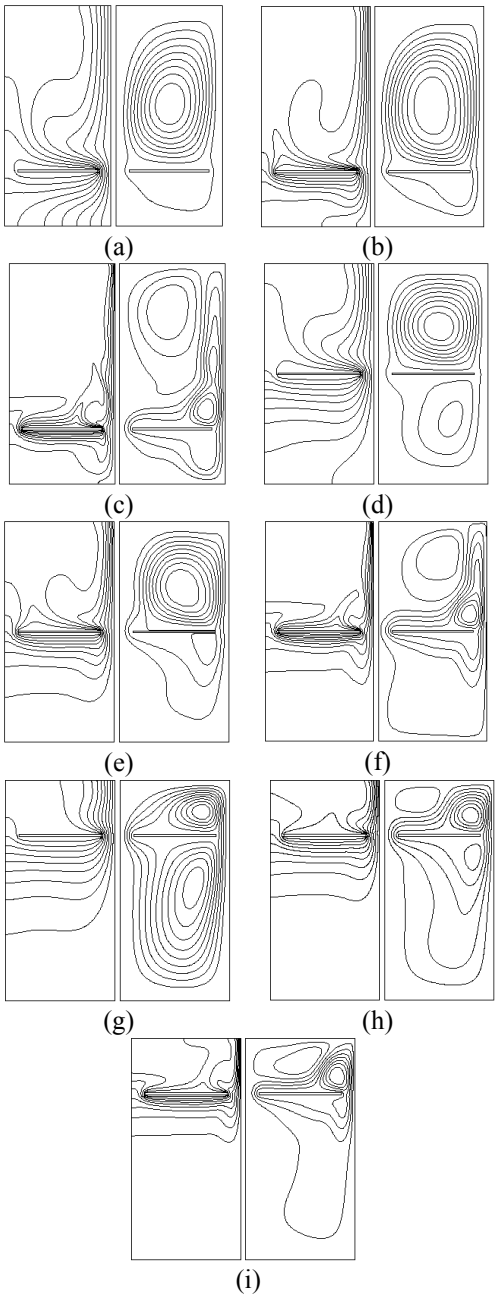

Figure 6. Isotherms (left) and streamlines (right) for A=2 and ℓ/L=0.75, (a), (d), (g) Ra=10^5; (b), (e), (h) Ra=10^6; and (c), (f), (i) Ra=10^7 (For (a), (b), (c) Y_0=0.25, for (d), (e), (f) Y_0=0.5, and for (g), (h), (i) Y_0=0.75).

In Figure 6, the isotherms and the streamlines for A=2, ℓ/L=0.75, Ra=10^5, 10^6 and 10^7 are depicted for three plate locations. For Y_0=0.25, in Figures 6(a), 6(b) and 6(c), the main circulation is basically established in the section above the isothermal plate due to blockage effect of a wider isothermal plate. However, as Rayleigh number increases, the roll encompassing the plate is strengthened. Thermal boundary layers, along side the cold wall and the plate, are distinctly observed. For increasing Rayleigh number, the boundary layers become thinner which yield increased heat transfer rates. For Ra=10^7 in Figure 6(c), as the streamlines shrink to cover the isothermal plate, the circulation is confined mainly to the right hand side of the enclosure. A strong counter-clockwise roll established at the upper-left corner of the enclosure pushes the detached plume from the top of the plate towards the cold wall. For the plate location Y_0=0.5, in Figures. 6(d), 6(e) and 6(f), the main circulation runs around the isothermal plate rather easily since the region below the plate remains cold. The boundary layer along the cold wall extends, again, from the top to the horizontal plate level. In Figures 6(g), 6(h) and 6(i), the isotherms and streamlines for plate location of Y_0=0.75 is depicted. In Figure 6(g), the main circulation encloses the plate; however, two clockwise rolls, one above and the other one below the plate, are established. The inner roll below the plate is stronger (Figures 6(g) and 6(h)). The thermal boundary layers are becoming slender in the vicinity of hot plate and cold wall which extends slightly down below the plate level. For Ra=10^7, Figure 6(i), a counter-clockwise roll at the upper left corner is formed shifting the main circulation towards the cold wall. For Ra=10^5, Figure 6(a), (d) and (g), a rising plume formations is not clear, indicating the domination of the conduction heat transfer on top wall of the plate. For higher Rayleigh number cases, a vertical plume is established and it is shifted towards the cold wall.

Figure 7 depicts, for A=2 and Ra=10^6, the local Nusselt number ($Nu_Y=\partial\theta/\partial X$) variation along the cold wall with respect to the plate length and location. For Y_0=0.25 and ℓ/L=0.5, the local Nusselt reaches a maximum in the vicinity of the top wall. It steadily declines along the cold wall towards the horizontal plate level; however, as seen in Figure 5(b), the local Nusselt number exhibits a slight increase due to the existence of a small roll (inside the main circulation) above the plate, pressing the descending air near the cold wall thereby reducing the thermal boundary thickness. Then, below the plate level, the local Nusselt number decreases towards the bottom of the cold wall where convection heat transfer diminishes. For ℓ/L=0.75 in Figure 6(b), since the gap between the plate and the cold wall is narrower, the thermal boundary layers are condensed at the exit of the gap which results in an increase in the local Nusselt number just below the horizontal plate level. Once the fluid passes through the gap between the plate and the cold wall, the local Nusselt number sharply declines towards the bottom of the cold wall. Similarly, for

Y_0=0.5 and ℓ/L=0.5 in Figure 5(e), the local Nusselt number starts with a maximum and decreases towards the horizontal plate level, but since inner roll above the plate still exists, the boundary layer thickness become slightly thinner along the cold wall above the horizontal plate level, causing more heat to be dissipated from this portion of the wall. On the other hand, for Y_0=0.5 and ℓ/L=0.75 in Figure 6(e), the gap between the horizontal plate and the cold wall is shorter; the thermal boundary layer at the cold wall tends to shrink below the plate due to an inner roll just below the isothermal plate. As a result, the local Nusselt number displays a peak around Y=0.45 and continues to decline sharply towards the bottom of the cold wall. For Y_0=0.75 and ℓ/L=0.5 in Figure 5(h), since thermal boundary layer is established from the top of the cold wall all the way down, the local Nusselt number is, as expected, maximum near the top wall, followed by a sharply decline as the fluid descends towards the bottom of the enclosure where the fluid reservoir is cold. For Y_0=0.75 and ℓ/L=0.75 in Figure 6(h), having a maximum near the top wall where the temperature gradients are the highest, the local Nusselt number sharply declines along the cold wall towards the horizontal plate level. The inner roll below the isothermal plate causes the boundary layers to shrink at the exit of the gap, thereby resulting in slight increase in heat dissipation around Y=0.7. Since the heat input of the system is provided through the isothermal plates, longer the plate length provides higher the heat input to the system. For that reason, the local Nusselt number profiles for ℓ/L=0.75 depict more heat dissipation from the cold wall than those of ℓ/L=0.5.

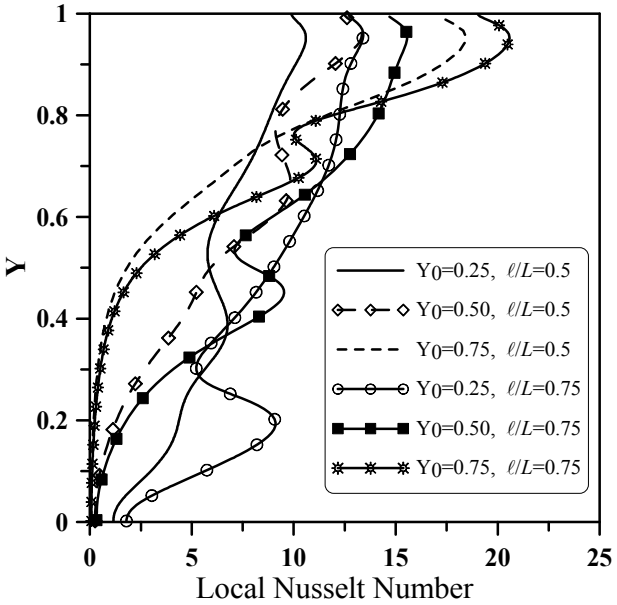

Figure 7. Local Nusselt number variation along the cold wall with respect to plate length and location for A=2 and Ra=10^6.

Heat Transfer Characteristics and Correlations

For square enclosures, the mean Nusselt number is plotted in Figure 8 as a function of Rayleigh number, the plate length (ℓ/L=0.5 and 0.75) and location (Y_0). For ℓ/L=0.5 case, the mean Nusselt number increases with increasing Rayleigh number. The mean Nusselt number is maximum for the isothermal plate which is located at Y_0=0.25. As the plate is vertically elevated to Y_0=0.5 position, the mean Nusselt number decreases only slightly for Ra<10^7. However, as the plate is raised to a higher location, such as Y_0=0.75, the mean Nusselt number decreases sharply due to the disappearance of the Archimedes forces leading to expanding boundary layer below the horizontal level of the plate. For the plate length of ℓ/L=0.75, the mean Nusselt number, similar to ℓ/L=0.5 case, is maximum when the isothermal plate is located at Y_0=0.25, and it is minimum at Y_0=0.75 for all Rayleigh values. The mean Nusselt number for Y_0=0.25 and Y_0=0.5 locations are identical for Ra<10^6; however, for higher Rayleigh values, the mean Nusselt number for Y_0=0.5 case decreases only slightly.

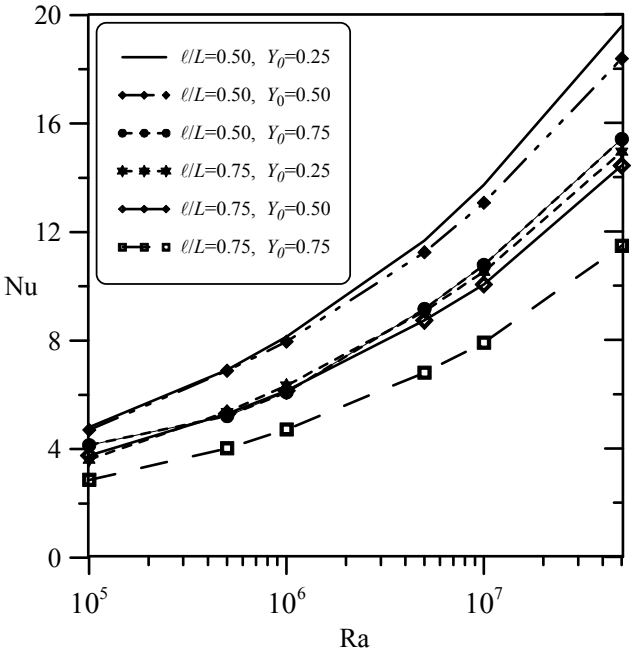

Figure 8. The mean Nusselt number variation in square enclosures as a function of Rayleigh number, plate length and locations.

In Figure 9, the mean Nusselt number for rectangular enclosure (A=2) is plotted as a function of Rayleigh number, the plate length (ℓ/L=0.5 and 0.75) and location (Y_0). In this case, the Nusselt number also increases with increasing Rayleigh number due to increased temperature gradients along the hot and cold walls. Similar to the square enclosures, the highest heat transfer is obtained for the plate location at Y_0=0.25, and the mean Nusselt number decreases with an increase in plate length. For Y_0=0.5 and ℓ/L=0.5, the mean Nusselt number decreases slightly in comparison to Y_0=0.25 location since the circulations around the isothermal plate get stronger and the removal of the hot fluid from the plate is relatively easy. For Y_0=0.75 and ℓ/L=0.5, the mean Nusselt number up to Ra=10^6 remains almost the same with that of Y_0=0.5 case but decreases

considerably for Ra>10^6. This is due to the formation of a plume with a wide base above the plate which, in turn, reduces the convective heat transfer from the top wall of the plate. For ℓ/L=0.75 plate length, the mean Nusselt number exhibit similar behavior to ℓ/L=0.5 case; that is, the mean Nusselt number increases with increasing Rayleigh number and decreases for increasing plate location (Y_0). However, the mean Nusselt number for Ra<10^6 is slightly higher in Y_0=0.5 than Y_0=0.25 location. For the same reasons mentioned above, the minimum of the mean Nusselt number is observed for Y_0=0.75 case for all Rayleigh values.

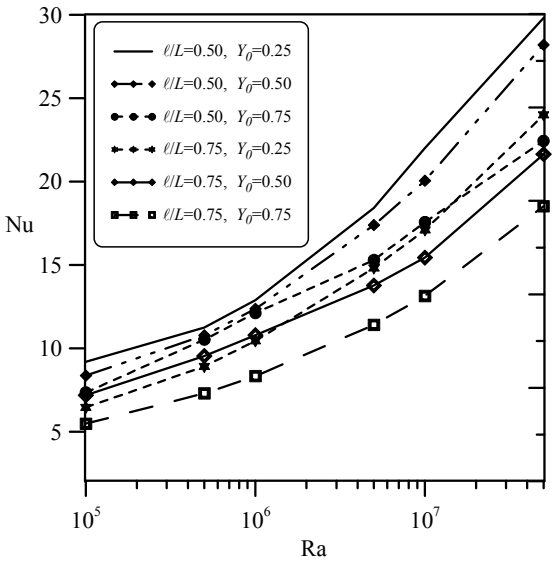

Figure 9. The mean Nusselt number variation in rectangular (A=2) enclosures as a function of Rayleigh number, plate length and locations.

In this study, the steady state mean Nusselt numbers for a range of Rayleigh numbers, the dimensionless plate locations (Y_0= y_0/H), the plate length parameter (ℓ/L) and the aspect ratios ($1 \le A \le 2$) were computed and recorded. The computed Nusselt data was correlated through multivariate regression for the following parameter ranges: $10^5 \le Ra \le 10^7$, $0.25 \le Y_0 \le 0.75$, $0.5 \le \ell/L \le 0.75$. The following correlation (r^2=0.9724) was obtained:

$$\mathrm{Nu} = 0.2354\mathrm{Ra}^{0.2085} A^{0.752} Y_0^{-0.223} \left(\frac{L}{\ell}\right)^{0.543} \qquad (7)$$

CONCLUSIONS

This parametric numerical study concludes the following. For increasing Rayleigh number, the velocity field becomes more violent and as a result the boundary layers get thinner which in turn yield higher heat transfer rates. As the plate length ℓ is increased from 0.5L to 0.75L, the Nusselt number decreases by about 20-25% since the flow field around the plate is relatively hindered due to a wider plate. The maximum heat transfer rate is obtained when the plate is located near the bottom of the enclosure (Y_0=0.25) since the space above the plate allows easy removal of the hot fluid from the plate. Due to the same reason, the plate location Y_0=0.5 results in slightly smaller mean Nusselt number. However, for Y_0=0.75, the mean Nusselt values decreases by 25-30% in comparison to Y_0=0.25 cases due to thermal stratification above the plate. As a result of this study, a correlation for the mean Nusselt number was obtained as a function of Rayleigh number, aspect ratio of the enclosure, plate length and location.

NOMENCLATURE

g	Earth's gravitational acceleration [m/s^2]
ℓ	Length of the plate length [m]
N	normal direction
t	time [s]
u, v	components of the fluid velocity [m/s]
x, y	coordinate axes [m]
x_0 , y_0	isothermal plate location [m]
A	aspect ratio [A=H/L]
H	enclosure height of [m]
L	length of enclosure [m]
Nu	mean Nusselt number [Eq. (6)]
P	pressure [Pa]
Pr	Prandtl number [$= \nu/\alpha$]
Ra	Rayleigh number [$= g\beta H^3 (T_h - T_c)/\alpha\nu$]
T	temperature [K]
U, V	dimensionless velocity components
X, Y	dimensionless axes
X_0, Y_0	dimensionless plate location [$= (x_0, y_0)/H$]

Greek Symbols

α	thermal diffusion coefficient [m^2/s]
β	volumetric thermal expansion coefficient[K^{-1}]
δ	plate thickness [m]
ρ	fluid density [kg/m^3]
θ	dimensionless temperature
ν	kinematic viscosity [m^2/s]
ψ	stream function [m^2/s]
Ψ	dimensionless stream function
τ	dimensionless time
ζ	vorticity

Subscripts

c	cold
h	hot

REFERENCES

Altaç, Z. and Kurtul, Ö., Natural convection in tilted rectangular enclosures with a vertically situated hot plate inside, *Applied Thermal Engineering* 27, 1832–1840, 2007.

Barozzi, G. S., Corticelli, M. A. and Nobile, E., Numerical simulation of time-dependent buoyant flows in an enclosed vertical channel, *Heat and Mass Transfer* 35, 89-99, 1999.

Barozzi, G. S. and Corticelli, M. A., Natural convection in cavities containing internal sources, *Heat and Mass Transfer* 36, 473-480, 2000.

Ben-Nakhi, A. and Chamkha, A. J., Effect of length and inclination of a thin fin on natural convection in a square enclosure, *Numer Heat Transfer*, *Part A* 50, 389-407, 2006.

Bessaih, R. and Kadja, M., Turbulent natural convection cooling of electronic components mounted on a vertical channel, *Applied Thermal Engineering* 20,141-154, 2000.

Bilgen, E., Natural convection in cavities with a thin fin on the hot wall *Int. J. Heat and Mass Transfer* 48, 3493–3505, 2005.

Bilen, K., Yapici S., Celik C.. A Taguchi approach for investigation of heat transfer from a surface equipped with rectangular blocks. *Energy Convers Manage* 42, 951–961, 2001.

Comini, G., Cortella, G. and Manzan, M., A stream function-vorticity-based finite-element formulation for laminar-convection problems, *Numer Heat Transfer, Part B* 28, 1-22, 1995.

Dağtekin, I. and Öztop, H. F., Natural convection heat transfer by heated partitions, *Int. Commun Heat Mass Transfer* 28, 823-834, 2001.

Desai, C. P., Vafai, K. and Keyhani, M., On the natural convection in a cavity with a cooled top wall and multiple protruding heaters, *J Electronic Packaging* 117, 34-45, 1995.

El Alami, M., Najam, M., Semma, E., Oubarra, A. and Penot, F., Electronic components cooling by natural convection in horizontal channel with slots, *Energy Conversion and Management* 46, 2762-2772, 2005.

Frederick, R. L. and Valencia, A., Heat transfer in a square cavity with a conducting partition on its hot wall, *Int. Commun. Heat Mass Transfer* 16, 347-354, 1989.

Heindel, T. J., Ramadhyani, S. and Incropera, F. P., Laminar natural convection in a discretely heated cavity: I-Assessment of three-dimensional effects, *ASME J Heat Transfer* 117, 902-909, 1995.

Heindel, T. J., Ramadhyani, S. and Incropera, F.P., Laminar natural convection in a discretely heated cavity: II- Comparisons of experimental and theoretical results, *ASME J Heat Transfer* 117, 910-916, 1995.

Incropera, F.P., Convection heat transfer in electronic equipment cooling. *ASME J Heat Transfer* 110, 1097-1111, 1988.

Kang, B. H. and Jaluria, Y., Natural convection heat transfer characteristics of a protruding thermal source located on horizontal and vertical surfaces, *Int. J. Heat Mass Transfer* 33, 1347-1357, 1990.

Le Quéré, P., Accurate solutions to the square thermally driven cavity at high Rayleigh number, *Computers and Fluids* 20, 29-41, 1991.

Markatos, N. C. and Pericleous, K. A., Laminar and turbulent natural convection in an enclosed cavity, *Int. J. Heat Mass Transfer* 5, 755-772, 1984.

Patankar, S. V., *Numerical Heat Transfer and Fluid Flow*, Hemisphere Publishing Corporation, Washington DC, 1980.

Türkoğlu, H. and Yücel, N., Natural convection heat transfer in enclosures with conducting multiple partitions and side walls, *Heat and Mass Transfer* 32, 1-8, 1996.

Sun, Y. S. and Emery, A. F., Effects of wall conduction, internal heat sources and an internal baffle on natural convection in a rectangular enclosure, *Int. J Heat Mass Transfer* 40, 915-929, 1997.

Sathe, S. B. and Joshi, Y., Natural convection liquid cooling of substrate-mounted protrusion in a square enclosure: effects of thermophysical properties, geometric dimensions and boundary conditions, in: R.A. Wirtz, G.L. Lehmann (Eds.), *Thermal Modelling and Design of Electronic Systems and Device*, Vol. HTD 153, ASME (1990) 73-80.

Yücel, N. and Türkoğlu, H., Numerical analysis of laminar natural convection in enclosures with fins attached to an active wall, *Heat and Mass Transfer*, 33(4), 307-314, 1998.

Vahl Davis, G. D., Natural convection of air in a square cavity: a bench mark numerical solution, *Int. J. Numer Method Fluids* 3, 249-264, 1983.